Scientific Research Publishing

World Journal of Engineering and Technology, 2024, 12, 24-39
https://www.scirp.org/journal/wjet
ISSN Online: 2331-4249
ISSN Print: 2331-4222

Development and Validation of a Scaled Electric Combat Vehicle Tire Model

Haniyeh Fathi, Aricha Mehrotra, Zeinab El-Sayegh*

Department of Automotive and Mechatronics Engineering, Ontario Tech University, Oshawa, Canada
Email: *Zeinab.el-sayegh@ontariotechu.ca

How to cite this paper: Fathi, H., Mehrotra, A. and El-Sayegh, Z. (2024) Development and Validation of a Scaled Electric Combat Vehicle Tire Model. *World Journal of Engineering and Technology*, **12**, 24-39.
https://doi.org/10.4236/wjet.2024.121002

Received: November 20, 2023
Accepted: January 1, 2024
Published: January 4, 2024

Abstract

Pneumatic tire modeling and validation have been the topic of several research papers, however, most of these papers only deal with pneumatic passenger and truck tires. In recent years, wheeled-scaled vehicles have gained lots of attention as a feasible testing platform, nonetheless up to the authors' knowledge there has been no research regarding the use of scaled tires and their effect on the overall vehicle performance characteristics. This paper presents a novel scaled electric combat vehicle tire model and validation technique. The pro-line lockdown tire size 3.00 × 7.35 is modeled using the Finite Element Analysis (FEA) technique and several materials including layered membrane, beam elements, and Mooney-Rivlin for rubber. The tire-rim assembly is then described, and the rigid body analysis is presented. The tire is then validated using an in-house custom-made static tire testing machine. The tire test rig is made specifically to test the pro-line tire model and is designed and manufactured in the laboratory. The tire is validated using vertical stiffness and footprint tests in the static domain at different operating conditions including several vertical loads. Then the tire is used to perform rolling resistance and steering analysis including the rolling resistance coefficient and the cornering stiffness. The analysis is performed at different operating conditions including longitudinal speeds of 5, 10, and 15 km/h. This tire model will be further used to determine the tractive and braking performance of the tire. Furthermore, the tire test rig will also be modified to perform cornering stiffness tests.

Keywords

Tire Modeling, Tire Testing Machine, Vehicle Dynamics, Unmanned Vehicle Modeling, Finite Element Analysis, Tire Mechanics

1. Introduction

The development of military vehicles over the last few decades and recent litera-

ture on multi-steerable mobile platforms both point to a lack of effort in this combined sector to pursue sophisticated technology. As a result, in 2019, Tan *et al.* [1] designed and created a revolutionary 1:6-sized electric battle vehicle prototype with eight independently powered and steerable wheels as shown in **Figure 1**. This vehicle serves as a research platform for the authors' research group. The vehicle is used to conduct autonomous algorithms and techniques, in addition to vehicle dynamics work and virtual vehicle modeling.

The goal of this study was to develop a scaled model for upcoming studies on the navigation and control of autonomous vehicles in off-road environments. Tan *et al.* explained the development of the chassis, suspension, driving, and steering systems in depth, beginning with the mechanical design. Custom nodes and topics made for hardware communication are used to construct the electronics required for vehicle actuation within the Robot Operating System. To enable autonomous navigation, path planning, and obstacle avoidance capabilities are employed. The result of this effort is a robotic platform that is fully operational, instrumented, and has a modular software architecture. Analysis of the vehicle's design, performance, and autonomous navigational capabilities have all undergone positive trial testing. The aluminum chassis is shaped like the letter T and is constrained by the weight and size requirements as it complies with the suspension configuration. It is the scale of the vehicle that factors such as vibration and aerodynamics are neglected due to scaled size. The Scaled Electric Combat Vehicle (SECV) was confirmed to be a completely working prototype with a high potential for upcoming autonomous navigation study based on the findings of both types of testing.

2. Literature Review

In 2023, Sidhu *et al.* [2] compared the structural rigidity of the non-pneumatic tire's (size 15/6N6) features of the wheel to the circumstances of the collision. Finite Element Analysis (FEA) was used in this investigation to create a model of the non-pneumatic interaction between tires and roads. The non-pneumatic tire analytical model was then verified in static and dynamic reactions employing several simulated tests. The verified non-pneumatic tire was then used to investigate tire-road interaction characteristics. The features of the tire-road interaction were then assessed using a rolling resistance test under various operating conditions. The effectiveness of tires would rise if this study were to be successful while enabling a deeper comprehension of the behavior of non-pneumatic tires under various contact circumstances.

In 2021, Phromjan *et al.* [3] investigated the efficiency of a tire while supporting a compressive load, and a solid tire model of a forklift was designed. To analyze the stress-strain characteristics, rubber compounds for solid tires were tested. For showing these characteristics in all layers of solid tires, the Ogden model was found suitable. The 3D model was developed by assembling the internal, middle, and tread layers. This study provided an approach to determine a

Figure 1. Physical SECV Prototype [1].

constitutive model for those rubber compounds that are used to produce the 3-layer solid tire. Curve fitting was used to establish the three rubber compounds' constitutive models. The chosen Ogden model was fitted to the rubber compounds' stress-strain curves and compared the KOMACHI solid tire footprints obtained from simulations of the FEM model with full tire trials.

In 2020, Suvanjumrat *et al.* [4] designed a Non-Pneumatic (NP) tire model for ride comfort evaluation. The ideal design of the NP tire has a load-carrying capacity, and the vertical stiffness can be easily achieved utilizing the static finite element method (FEM) with an appropriate material model. The study aimed to design a FEM to learn about the dynamic characteristics and analyze the ride comfort property of the NP tire. The FEM of the NP tire consisted of tread bands and spokes that were taken to model the steel belt layers of the NP tire. The findings were compared to analyze the model's validity in capturing critical dynamic characteristics that were thought beneficial in building the NP tire to have ride quality that challenged the generally used pneumatic tire.

In 2020, Phromjan *et al.* [5] analyzed the tire-rotating behavior by using the drum testing method to improve tire performance, rolling resistance, and contact force. The cylindrical drum was used to test the tire in an indoor laboratory. Therefore, the contact patch of a solid tire rolling on a drum surface ought to produce findings equivalent to those of tire testing on a flat surface. It was concluded that the solid tire model's contact patch and the pressure measuring film agreed. According to the statistics, the contact coefficient is identical at 0.4. Thus, it can be inferred that the solid tire finite element model could replicate the contact patch on the curved surface and produce accurate results.

In 2019, El-Sayegh *et al.* [6] provided a new high lug farm service (HLFS) agricultural tire size 220/70B16 tread design that operates for off-road conditions. A hyper-elastic material that precisely demonstrates the mechanics and behavior of rubber used in tires, namely the Mooney-Rivlin material was used to construct the tire tread of HLFS. The manufacturer's provided data was then compared with the result obtained from the FEA analysis for validation purposes for several parameters such as radial, lateral, and tangential stiffness. The study then continued to study the HLFS tire efficiency over clayey loam for different operating conditions. The first validation test showed the vertical deflection

performed on a hard surface. It was noticed that the highest displacement was recorded in the lower wall which is closest to the contact surface. In addition, as the vertical stiffness increases, the inflation pressure increases past the operating inflation pressure for the tire.

This paper focuses on the development and validation of pro-line lockdown tire size 3.00 × 7.35. The tire is modeled using finite element analysis and several material properties. In addition, a custom-made static testing machine is manufactured to validate the tire model. Furthermore, tire-road interaction characteristics including rolling resistance and cornering stiffness are evaluated. This paper provides a novel approach to scaled electric combat vehicle tire dynamics. The findings of this paper provide insights into modeling and evaluating non-standard tire-terrain interaction.

3. Research Methodology

This section presents the research methodology selected for the testing and modeling of the tire model. The methodology highlights two main aspects the tire testing machine which is custom-made for the scaled tire and the FEA technique used to model the tire.

3.1. Tire Testing Machine

In order to determine the tire characteristics a model of the tire test rig was first designed in CAD software and then tests were done on it to ensure the strength and rigidity of the modeled rig. This section presents the test rig design and manufacturing, in addition to the tire test rig validation.

3.1.1. Tire Rig Design and Manufacturing

The test rig was built with a variety of parts, the design's goal was to quantify the force caused by the deflection of the tire in order to determine the vertical stiffness. The project's concept-generating phase was put into action following consideration. The tire was fixed at the required deflection position using the test rig. The tire could only move vertically, both its lateral and longitudinal movements were constrained. This necessitated the existence of columns on the tire's two sides, which the aluminum extrusions made possible. The vertical deflection test also required that the whole test equipment remain stationary. As a result, the test rig with a fixed framework was created. Both powder and ink solutions were examined for the footprint test, but the powder was chosen since it was simpler to clean the tire after testing. In addition, there was only one spare tire, and any substance that stayed on the tire would have impacted the precision of subsequent tests. During various stages, tools including a 3D scanner, measuring tape, drills, screws, and other mechanical parts were employed.

The first step of the design involved compiling experimental data from several experiments that were carried out on the actual tire. The problem was divided into two portions so that the outcomes of the two approaches could be compared to verify the FEA tire model. The test rig's approach involved measuring

the response force, and examining the tire's static footprint when it was subjected to constant vertical deflection. The test rig shown in **Figure 2** was created to suit several requirements to complete this mission. It was a stiff construction with a little structural deflection as the first movement while being tested. The vertical stiffness test was a very sensitive test whose accuracy depended on a variety of variables. The rig's downward deflection caused the tire to react by applying a normal force in the opposite direction. The tire and the two sliding assemblies remained aligned to the vertical z-axis throughout the testing to uniformly distribute the load throughout the tire because the test was solely concerned with the vertical stiffness of the tire.

The second part of the test apparatus was the procedure for applying the vertical load to the tire. The force's potential uses were outlined in the idea generation. The team's suggestions covered a variety of innovative approaches, from using weights to load the tire to using a motor to produce torque to using a rack and pinion setup to provide the vertical force. The rig was designed to generate downward forces of at least 50 N and comfortably exceed 250 N.

Following the application of white powder to the basin for color contrast, the tire was lowered into the basin while displacement testing was performed, causing the white powder to push against the tire. The contact surface allowed for good visualization of the tire footprint (once the tire was undeformed and returned to its normal location). The length and width of the resultant contact patch were evaluated after each footprint test, and the basin was properly cleaned. Considering the different deflection points with the test rig, resulted in different contact patches and profiles. It was later concluded that the footprint would expand as the downward deflection of the tire increased.

3.1.2. Test Rig Calibration and Validation

Several components of the test rig had to be tested and calibrated, including the force transducers and the multimeter. Based on the pre-defined data set, it was known that the resting voltage (meaning no force applied) of the multimeter was approximately 1.4 millivolts. With this in connection to the force transducer, intuitively, as the transducer was loaded more, the voltage increased. However, the setup of the test rig had some features to consider when loading the force transducer. First was that the brake kit subassembly, when calibrating the voltage, was always pushing down on the force transducer. So, this needed to be accounted for when calibrating the voltage to the force. To do this, the brake kit was weighed on a scale in kilograms and converted to newtons of force.

The calibration test was conducted with an item placed on the beam of the brake kit, weighing down on the force transducer as shown in **Figure 3**. The data collected from the transducer was then used for coloration as shown in **Figure 4**.

The contents of the graph shown in **Figure 4** indicated that the calibration was a success. The correlation coefficient R2 was equal to one, this value acts as a ratio of correlation between the x-axis (voltage) and y-axis (force) and ranges from 0 - 1. A correlation coefficient of 1 means that the data is perfectly

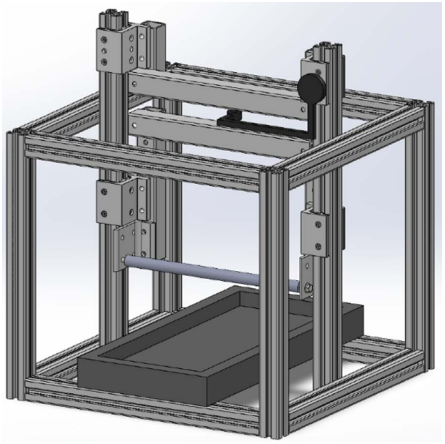

Figure 2. Final test rig design model.

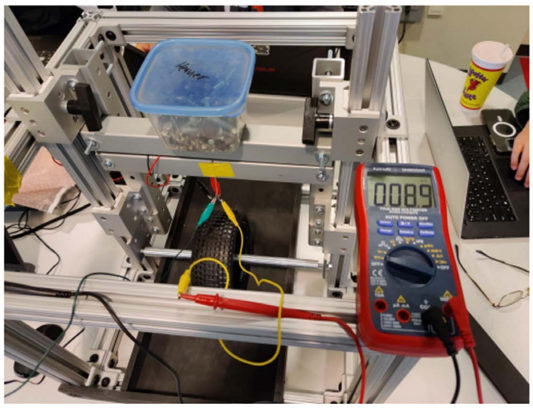

Figure 3. Nail Box 2 millivolt measurement.

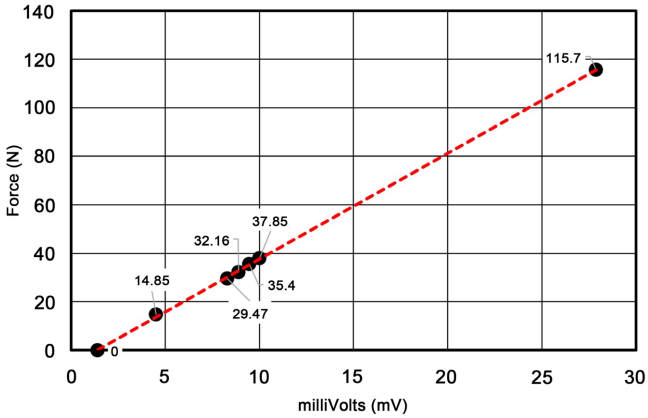

Figure 4. Calibration test graph.

correlated and thus linear. This calibration was significant in making sure that the group had the proper readings when conducting the experiment.

3.1.3. Test Rig Measurement Data

The vertical stiffness test plan included imparting a known displacement to the tire and measuring the force exerted by the tire assembly on the force transduc-

er. The force exerted by the tire assembly was measured using the force transducer assembly, which produced a millivolt reading that was shown on the multimeter and corresponded to a set force in Newtons. Using the calibration test described above, the calibration graph was used to establish the known link between millivolt measurement and the force observed. Ten vertical stiffness tests were performed. The results of the tests were entered into an Excel spreadsheet, and for each test, a force versus displacement graph was constructed, the slope of which represented the vertical stiffness of the tire for that test. After all, testing was completed and all data was collected and displayed as shown in **Figure 5**, ten vertical stiffness values were computed, with the average being computed. The measured vertical stiffness of the tire was then taken as the average vertical stiffness value.

Based on the results obtained from the average of the 10 different vertical stiffness tests the vertical stiffness is calculated to be 21.24 N/mm.

The contact patch test, at times, referred to as the tire footprint test, was the tire's second important test. This test's objective was to examine the tire's interactions with a contact surface. The weight of the vehicle pushing the round tires on the ground creates the contact patch. The treads of a tire are designed to deflect and create these contact areas. The test rig was used to duplicate this, and it was built using the Proline lockdown tire's specifications (187 mm × 81 mm). A sample of the test procedure and visual results are shown in **Figure 6**.

The tire was loaded to displacement points 8, 14, and 18. The white powder was used in contrast to the black plywood basin, which gave more visual clarity when conducting the test. The results of the footprint test for 6 different tests are presented in **Table 1**.

It is noticed that as the vertical displacement increases the contact area of the tire increases as well, which is expected due to the increase in vertical load.

3.2. FEA Tire Modeling

In this research a pro-line Lockdown S2 tire [7] was chosen and modeled using Finite Element Analysis (FEA) in Pam-Crash software. Pro-line racing is a US based tire manufacturer which specializes in manufacturing tires and wheels for radio-controlled off-road vehicles. Pro-line tires were used with autonomous scaled electric combat vehicle shown in **Figure 1**. Moreover, the lockdown S2 tire is 1:5 scale tire made using pro-line S2 compound. The initial model of the Proline tire was generated using a Scale method in Pam-Crash software as shown in **Figure 7**. To calibrate the FE model of the pro-line tire, a vertical steady state load of 85 N was applied to the center of tire. Moreover, to inflate tire, an inflation pressure of 7200 Pa applied to the tire circumferential direction in the inner cavity of tire.

Moreover, the total termination time of the simulation was set to 1 second. Furthermore, gravity was defined as a structural load in the acceleration field using a curve function with the value of 9.81 m/s^2. Additionally, all the details are fully explained in the next sections. Several FEA tests were performed

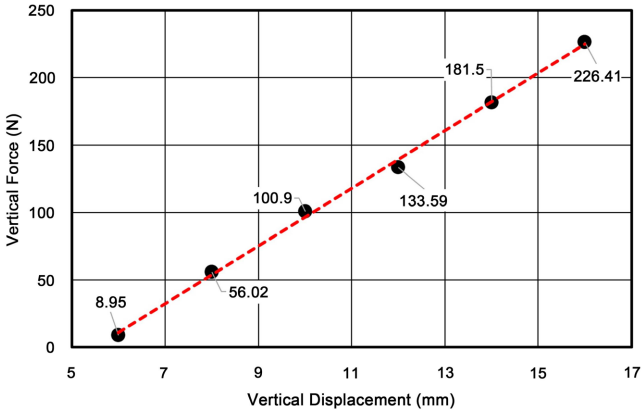

Figure 5. Sample of vertical stiffness test graph.

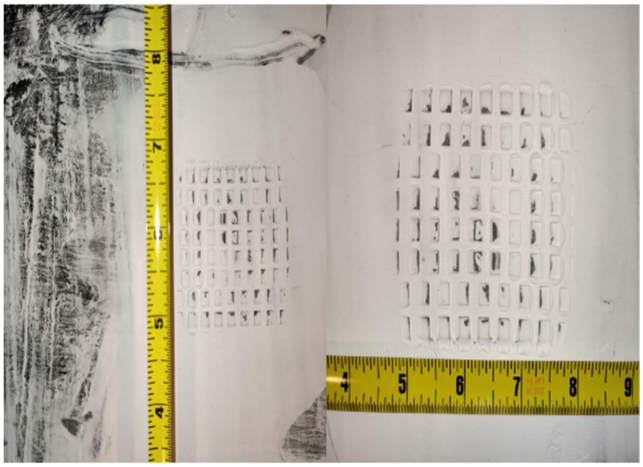

Figure 6. Sample of the contact length and width.

Table 1. Footprint data collected at different displacements.

Test Set	Displacement Point	Length (mm)	Width (m)
1	4	40.64	46.99
2	4	41.27	44.45
3	7	63.5	45.72
4	7	63.5	44.45
5	9	79.37	47.62
6	9	79.37	45.08

including vertical stiffness and footprint test to simulate tire behavior and compare the results with the experimental Rig test data.

3.2.1. Tire Materials

To simulate a tire model which is capable of representing the actual tire behavior, the pro-line tire was modeled using various layers and reinforcements. The compound used for the pro-line tire is optimized for high wear resistance in temperature around 80-degree Fahrenheit.

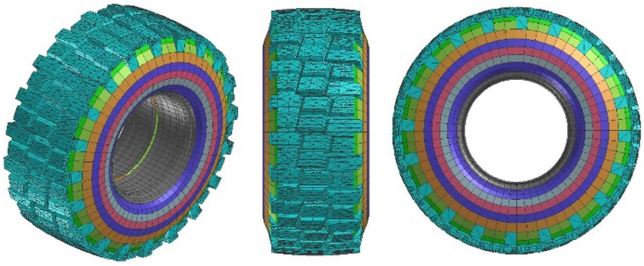

Figure 7. FE model of the Pro-Line tire in Pam-Crash software.

Many polymers and elastomers, particularly those used in tire structure can be modeled using isotropic hypereasticity [8]. To model tire compound, the Mooney-Rivlin model was implemented which is an expansion of the Neo-Hookean model based on the strain energy density function [9].

For the Mooney-Rivlin model, the Cauchy stress can be represented as Equation 1 [10].

$$\sigma = \frac{2}{J}\left(C_{10} + C_{01}I_1^*\right)b^* - \frac{2C_{01}}{J}\left(b^*\right)^2 + \left[k\left(J-1\right) - \frac{2I_1^*C_{10}}{3J} - \frac{4I_2^*C_{01}}{3J}\right]I \quad (1)$$

While $k \to \infty$, the incompressible version of the Mooney-Rivlin material is described as following Equations 2 - 4 [10];

$$\sigma_{uniax} = 2\left(\lambda^2 - \frac{1}{\lambda}\right)\left[C_{10} + \frac{C_{01}}{\lambda}\right] \quad (2)$$

$$\sigma_{planar} = 2\left(\lambda^2 - \frac{1}{\lambda^2}\right)\left[C_{10} + C_{01}\right] \quad (3)$$

$$\sigma_{biaxial} = 2C_{10}\left(\lambda^2 - \frac{1}{\lambda^4}\right) + 2C_{01}\left(\lambda^4 - \frac{1}{\lambda^2}\right) \quad (4)$$

The above equations express the Cauchy stresses in the uniaxial, planar, and equi-biaxial deflections, respectively [10]. Furthermore, the first (loading) and second (loading) Mooney-Rivlin law coefficients, are represented by C_{10} and C_{01}, respectively. Consequently, the total Finite Element model of the pro-line tire was simulated using 20 number of layers as shown in **Figure 8**.

3.2.2. FEA Tire Model

The inside of the lockdown S2 tire consists of detailed webbing which strengthens the tire carcass and limits excessive tire expansion. To create a finite element model of the Lockdown S2 pro-line tire, the model was scaled to achieve the desired dimension. Pro-line tire dimensions according to the manufacturer's website [7] are with 81 mm width and a height of 187 mm.

The total weight of tire body including the rim was 0.635 kg which was calibrated using the density optimization method of the various layers of tire structure. The final FE tire model consists of a total of 9923 nodes and 16280 elements. Some of the rubber-liked materials in the tire including tread base, shoulder, and sidewall were meshed using 7140 three-dimensional solid hybrid incompressible continuum elements revealing the isotropic hyperelastic behavior.

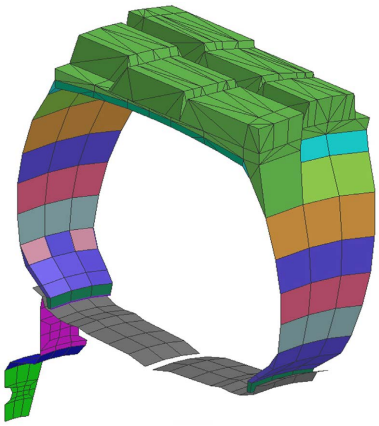

Figure 8. Tire cross-sectional view after meshed definition procedure.

Particularly, to mesh tread top and tread pattern, three-dimensional elements including 6140 elements of 4-Node Tetrahedral element were implemented. The reinforcement cords of tire and carcass plies were modeled using 2D thin shell elements and 2D membrane elements which reflect the linear elastic behavior. Moreover, beam elements also were used to mesh the cords and plies in the one-dimensional pattern. Furthermore, the rim was meshed using Shell elements.

3.2.3. Tire-Road Interaction

The lockdown S2 features an open tread pattern for increasing traction in loose conditions and connected side tread technology which reduces the edginess of the tire to prevent clipping of the tire under excessive side load forces. An appending approach was selected to generate the tire-terrain interaction model. For this purpose, firstly a rigid hard road surface was created and was meshed using fine thin shell elements to retain the interaction and contact of the tire contact patch nodes with the road nodes segments while rolling. Then, a constraint tie condition was defined with a thickness of 5 mm for the tire-road interface that tied the tire model to the road. Finally, the tire was appended to the meshed road surface as shown in **Figure 9**.

In order not to lose any contacts a node-to-segment contact algorithm [11] that includes edge treatment capability was implemented to simulate this interaction (without losing any contacts) in the straight rolling.

It must be noted that while adopting node-to-segment contact constraint, the entities are the tire that was selected as the slave body (Blue), and the other one is road was chosen as the main and master part (Green) as shown in **Figure 10**.

4. Results and Discussion

In this section, the tire model validation is static domain using vertical stiffness test and footprint test is presented. Furthermore, the tire-road interaction characteristics including the rolling resistance and cornering stiffness are evaluated and analyzed.

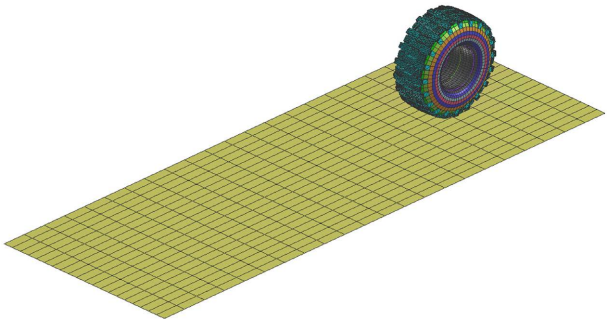

Figure 9. Appended tire model to the road surface.

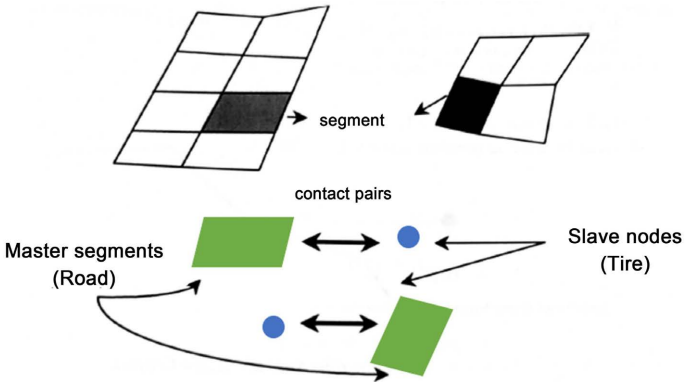

Figure 10. Contact definition for the node to segment in the Pam-Crash software [11].

4.1. Tire Model Validation

In the static domain, the tire is validated using vertical stiffness and footprint tests. The simulated results are then compared to the experimental data collected in this study.

4.1.1. Vertical Stiffness Test

In essence, during the vertical stiffness test, a ramp vertical load is applied to the tire center, and the tire's normal deflection in the vertical axis is measured. The vertical stiffness test was carried out in the advanced virtual environment software named Pam-Crash. In this case, the ramp load is set to a maximum value of 250 N, and the vertical deflection is recorded. After extracting the vertical deflection of the tire center and the vertical contact force between the tire and ground a graph representing the vertical load and a function of deflection is presented in Figure 11.

Figure 11 shows the variation of the vertical load as a function of vertical displacement. The graph shows a slight non-linear behaviour which is expected at high vertical loads. In order to estimate the vertical stiffness of the simulated tire a linear approximation is taken, and the slope of the line is regarded to as the stiffness. Based on the experiment work presented in Section 2.3, the vertical stiffness is 21.24 N/mm whereas the simulated vertical stiffness is 20.44 N/mm making a difference percentage of 3.8% which is well within the acceptable range.

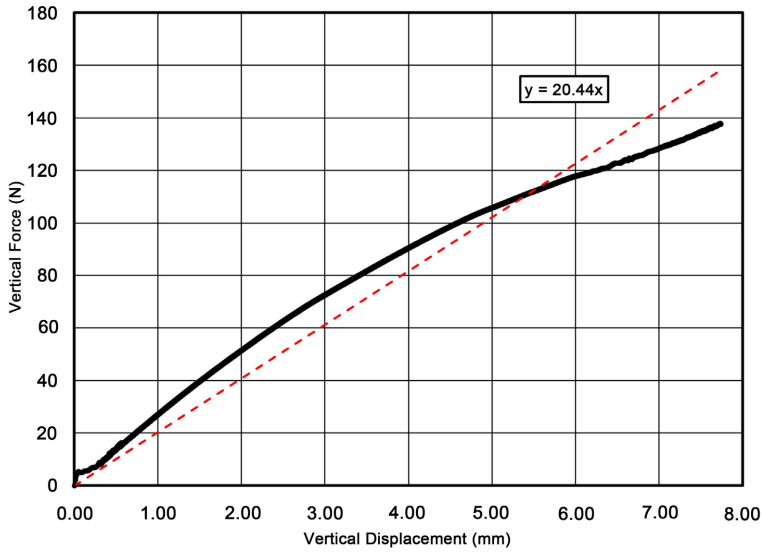

Figure 11. Vertical load as a function of vertical displacement.

Thus, the simulated tire is considered to have a similar behavior to the proline lockdown tire. This also indicates that the simulated tire vertical behavior is in good agreement with the actual model and that the FEA tire model can be used for ride comfort studies.

4.1.2. Footprint Test

During a static footprint test a constant vertical load is applied to the center of the tire and the tire contact with the ground (length and width) is calculated. The test is repeated for different vertical loads including 85, 149, and 191 N. Those vertical loads are selected to be equivalent to a vertical displacement of 4, 7, and 9 mm which are measured during the physical testing. **Figure 12** shows the contact patch of the proline tire with the ground at an 85 N applied vertical load. The recorded contact width was 48.5 mm, and the contact length was 47.2 mm.

Figure 13 shows the contact patch of the proline tire at an applied vertical load of 149 N. The recorded contact width was 48.5 and the contact length was 80.2 mm. It is noticed that as the vertical load increases the contact width increases as well, however, the contact length of the footprint patch almost remains constant as this represents the overall width of the tire.

Thus, comparing the results obtained from the footprint simulations test to those obtained from the physical footprint test, it can be concluded that the footprint results are in good agreement and within the acceptable error range of 9%. This indicates that the modeled FEA tire exhibits a similar contact area to the actual tire and can be used for further analysis of rolling and dynamic tire performance.

4.2. Tire-Road Interaction Evaluation

In this section, the tire-road interaction characteristics are described. The interaction characteristics include rolling resistance and cornering stiffness at

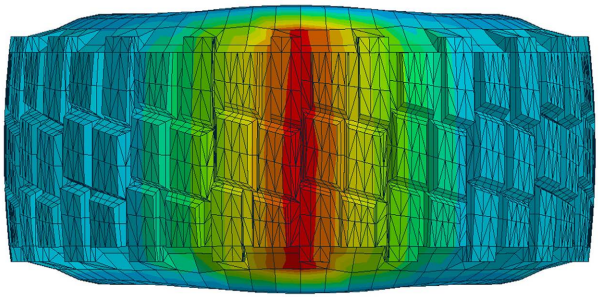

Figure 12. Footprint of the tire at 85 N applied vertical load.

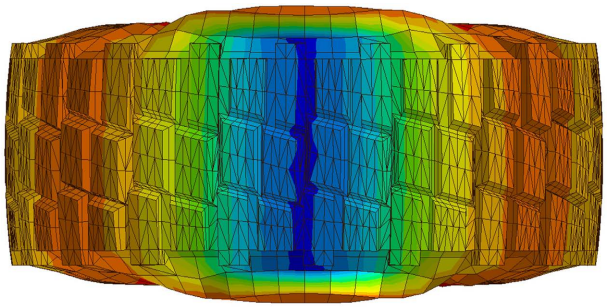

Figure 13. Footprint of the tire at 149 N applied vertical load.

different operating speeds ranging from 5 to 15 km/h which mimic the actual vehicle speed. In this case the study is done at 85 N vertical load which represents the vehicle weight on each tire.

4.2.1. Rolling Resistance Test

During a rolling resistance test, a constant vertical force is applied to the center of the tire, and the tire is allowed to rotate in the longitudinal direction. A constant linear velocity is applied to the center of the tire and the simulation continues until the tire reaches a steady state. Then, the longitudinal and vertical forces on the tire-road contact are extracted and the rolling resistance coefficient is computed.

Figure 14 demonstrates the variation of the rolling resistance coefficient as a function of longitudinal speed for the proline tire with 85 N applied vertical load. It can be seen that as the longitudinal speed increases the rolling resistance coefficient increases as well. The height recorded rolling resistance coefficient is around 0.0147 at 15 km/h longitudinal speed, while the lowest recorded rolling resistance coefficient is around 0.00458 at 5 km/h longitudinal speed.

4.2.2. Cornering Stiffness Test

During a cornering stiffness test, the tire is pre-steered to the desired slip angle. In this case, the tire is pre-steered to 2-degrees. A constant vertical load of 85 N is then applied to the center of the tire. The tire is allowed to settle on the road and a constant longitudinal speed is then applied to the tire center until the tire reaches a steady state. In a cornering stiffness test, the contact forces in longitudinal, lateral, and vertical directions are extracted.

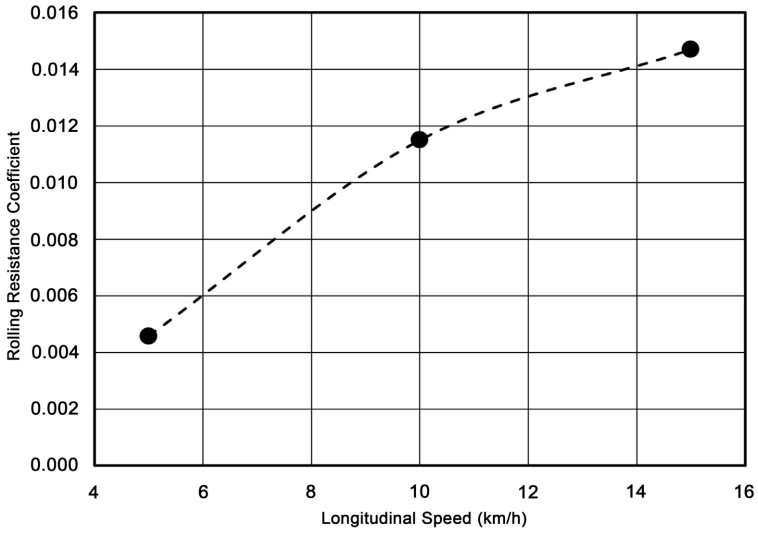

Figure 14. Rolling resistance coefficient as a function of longitudinal speed.

Figure 15 shows the variation of the contact forces as a function of the longitudinal speed for a tire during a 2-degree cornering test at 85 N applied vertical load. For both the lateral and longitudinal forces it can be seen that as the longitudinal speed increases both the contact forces increase as well. The cornering stiffness of a tire can be calculated using the relationship:

$$F_l = F_y \cos\alpha + F_x \sin\alpha \tag{5}$$

where F_x and F_y are the longitudinal and lateral forces, respectively; and α is the tire slip angle. The cornering stiffness can then be calculated by dividing the lateral force, F_l, by the slip angle.

Table 2 shows the calculated cornering stiffness and lateral force at different longitudinal speeds. It can be seen that the cornering stiffness increases as the longitudinal speed increases at a given vertical load. Overall, the cornering stiffness increases by about 11% when the tire speed triples from 5 to 15 km/h.

5. Conclusions

In this research, a lockdown S2 pro-line tire size 3.00 × 7.35 with 81 mm width and 187 mm was modeled and calibrated using Finite Element techniques. Several analyses were carried out to predict tire performance. For this pro-line tire, vertical stiffness, footprint test, Rolling Resistance test, and cornering test were performed. Finally, the output data were validated with the test Rig experimental data.

It was observed that the increase in vertical load applied to the tire center gives a rise in the vertical displacement of the tread pattern blocks in the tire-road contact patch. It is due to the large deformation of the tetrahedral tread blocks under the vertical static loading. This phenomenon also increases the contact patch area of the tire and the contact patch area in the Rig Test comes with the higher area with larger width and height of the tire track on the white powder in the test equipment container.

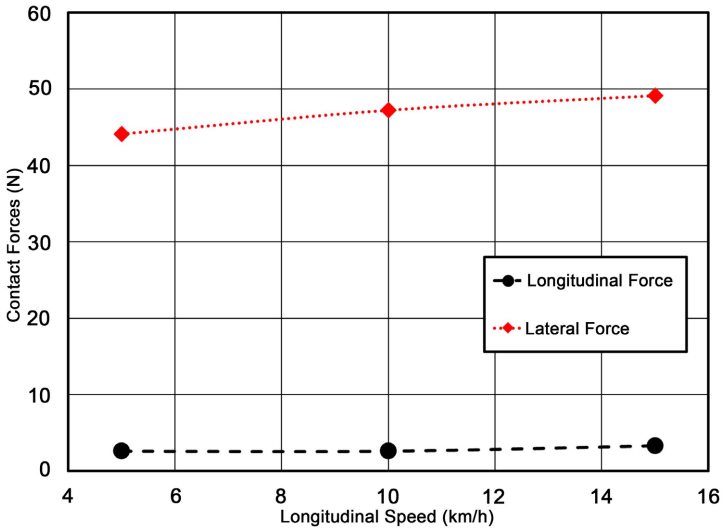

Figure 15. Contact forces as a function of longitudinal speed during a cornering test.

Table 2. Cornering stiffness at different longitudinal speed.

Speed (km/h)	F_l (N)	C_α (kN/rad)
5	44.16	5.06
10	47.26	5.41
15	49.18	5.63

From the rolling resistance test, it can be inferred that the increase in longitudinal linear speed of tire resulted in the higher rolling resistance coefficient regardless of the effect of temperature and material dissipation. This occurs due to the more traction of the tire tread blocks with the road in the higher speed as they interact with more nodes with the ground segments. An interesting finding about the cornering test is that the amount of tire longitudinal force, F_x was relatively remained stable in all speed. Moreover, it can be expressed from the results that tire linear speed has a negligible effect on the value of the tire contact force in the longitudinal direction (for this special case, pro-line tire). This can be proved by the small tire width and the tire size that might affect the tire forces.

Since the custom-made tire test rig was only designed to test for static analysis such as vertical stiffness and footprint, there was no way to validate the dynamic results such as the rolling resistance and cornering. Thus, the future work includes upgrading the tire test rig to include a motor and possibly drive the road and the tire to mimic a free rolling and driven tire cases. In addition, load cells will also be added to the tire test rig to measure contact forces and moments.

Conflicts of Interest

The authors declare no conflicts of interest regarding the publication of this paper.

References

[1] Tan, A.H., Lang, H. and El-Gind, M. (2019) A Novel Autonomous Scaled Electric Combat Vehicle. *International Design Engineering Technical Conferences and Computers and Information in Engineering Conference*, Anaheim, 18-21 August 2019. https://doi.org/10.1115/DETC2019-97163

[2] Sidhu, C.S., El-Sayegh, Z. and El-Gindy, M. (2023) Non-Pneumatic Tyre-Road Interaction Using Finite Element Analysis. *International Journal of Vehicle Systems Modelling and Testing*, **17**, 52-66. https://doi.org/10.1504/IJVSMT.2023.132314

[3] Phromjan, J. and Suvanjumrat, C. (2021) Development of Solid Tire Model for Finite Element Analysis of Compressive Loading. *Songklanakarin Journal of Science & Technology*, **43**, 229-236.

[4] Suvanjumrat, C. and Rugsaj, R. (2020) The Dynamic Finite Element Model of Non-Pneumatic Tire under Comfortable Riding Evaluation. *International Journal of GEOMATE*, **19**, 62-68. https://doi.org/10.21660/2020.76.9135

[5] Phromjan, J. and Suvanjumrat, C. (2020) The Contact Patch Analysis of Solid Tire on Drum Testing by Finite Element Method. *IOP Conference Series*: *Materials Science and Engineering*, **886**, Article ID: 012049. https://doi.org/10.1088/1757-899X/886/1/012049

[6] El-Sayegh, Z., *et al.* (2019) Development of an HLFS Agricultural Tire Model Using FEA Technique. *SN Applied Sciences*, **1**, Article No. 1454. https://doi.org/10.1007/s42452-019-1524-y

[7] https://www.prolineracing.com/pro-line/tires-and-wheels/

[8] Keerthiwansa, G.W.R., *et al.* (2018) Elastomer Testing: The Risk of Using Only Uniaxial Data for Fitting the Mooney-Rivlin Hyperelastic-Material Model. *Materiali in tehnologije*, **52**, 3-8. https://doi.org/10.17222/mit.2017.085

[9] Kim, B., *et al.* (2012) A Comparison among Neo-Hookean Model, Mooney-Rivlin Model, and Ogden Model for Chloroprene Rubber. *International Journal of Precision Engineering and Manufacturing*, **13**, 759-764. https://doi.org/10.1007/s12541-012-0099-y

[10] Bergström, J. (2015) Elasticity/Hyperelasticity. *Mechanics of Solid Polymers*, **2015**, 209-307. https://doi.org/10.1016/B978-0-323-31150-2.00005-4

[11] Group, E. (2000) Pam-Crash Theory Notes Manual. Pam System International.